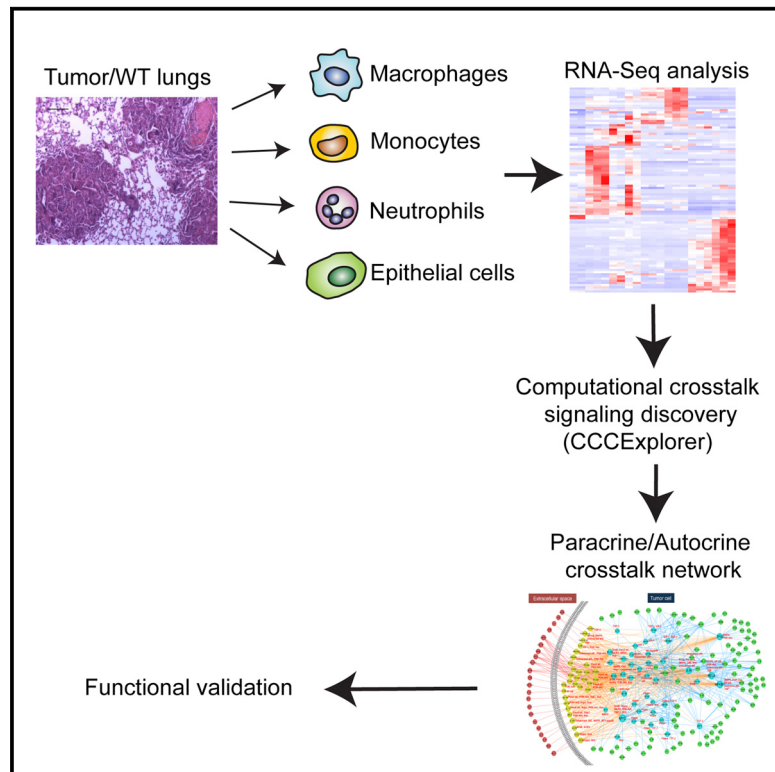


Transcriptome Analysis of Individual Stromal Cell Populations Identifies Stroma-Tumor Crosstalk in Mouse Lung Cancer Model

Graphical Abstract



Authors

Hyejin Choi, Jianting Sheng, ...,
Stephen T.C. Wong, Vivek Mittal

Correspondence

[\(S.T.C.W.\),](mailto:stwong@houstonmethodist.org)
[\(V.M.\)](mailto:vim2010@med.cornell.edu)

In Brief

The tumor-stroma crosstalk network in lung cancer is poorly understood. Choi et al. analyze cellular heterogeneity of stromal cells in *Kras*^{G12D/+}; *p53*^{-/-} lung cancer and identify the reprogrammed states of individual myeloid cells and tumor cells by RNA-seq analysis. The authors develop a computational model that identifies global paracrine/autocrine crosstalk networks.

Highlights

- Tumor microenvironment heterogeneity is analyzed in *Kras*^{G12D/+}; *p53*^{-/-} lung cancer
- RNA-seq identifies differentially expressed genes in stromal and epithelial cells
- A computational model is developed, identifying paracrine/autocrine crosstalk
- Computationally predicted crosstalk pathway is experimentally validated

Accession Numbers

GSE59831

Transcriptome Analysis of Individual Stromal Cell Populations Identifies Stroma-Tumor Crosstalk in Mouse Lung Cancer Model

Hyejin Choi,^{1,2,3,4,11} Jianting Sheng,^{8,11} Dingcheng Gao,^{1,2,3} Fuhai Li,⁸ Anna Durrans,^{1,2,3} Seongho Ryu,^{1,3,10} Sharrell B. Lee,^{1,2,3} Navneet Narula,⁶ Shahin Rafii,⁷ Olivier Elemento,⁵ Nasser K. Altorki,^{1,3} Stephen T.C. Wong,^{6,8,9,*} and Vivek Mittal^{1,2,3,*}

¹Department of Cardiothoracic Surgery

²Department of Cell and Developmental Biology

³Neuberger Berman Lung Cancer Center

⁴Weill Cornell Graduate School of Medical Sciences

⁵Institute for Computational Biomedicine, Department of Physiology and Biophysics

⁶Department of Pathology

⁷Ansary Stem Cell Institute and Department of Genetic Medicine

Weill Cornell Medical College of Cornell University, 1300 York Avenue, 525 East 68th Street, New York, NY 10065, USA

⁸Department of Systems Medicine and Bioengineering, Houston Methodist Research Institute, 6670 Bertner Avenue, Houston, TX 77030, USA

⁹Methodist Cancer Center, Houston Methodist Hospital, 6650 Fannin Street, Houston, TX 77030, USA

¹⁰Present address: Soonchunhyang Institute of Medi-bio Science (SIMS), Soonchunhyang University, Asan 336-745, Korea

¹¹Co-first author

*Correspondence: stwong@houstonmethodist.org (S.T.C.W.), vim2010@med.cornell.edu (V.M.)

<http://dx.doi.org/10.1016/j.celrep.2015.01.040>

This is an open access article under the CC BY-NC-ND license (<http://creativecommons.org/licenses/by-nc-nd/3.0/>).

SUMMARY

Emerging studies have begun to demonstrate that reprogrammed stromal cells play pivotal roles in tumor growth, metastasis, and resistance to therapy. However, the contribution of stromal cells to non-small-cell lung cancer (NSCLC) has remained underexplored. We used an orthotopic model of Kras-driven NSCLC to systematically dissect the contribution of specific hematopoietic stromal cells in lung cancer. RNA deep-sequencing analysis of individually sorted myeloid lineage and tumor epithelial cells revealed cell-type-specific differentially regulated genes, indicative of activated stroma. We developed a computational model for crosstalk signaling discovery based on ligand-receptor interactions and downstream signaling networks and identified known and novel tumor-stroma paracrine and tumor autocrine crosstalk-signaling pathways in NSCLC. We provide cellular and molecular insights into components of the lung cancer microenvironment that contribute to carcinogenesis. This study has the potential for development of therapeutic strategies that target tumor-stroma interactions and may complement conventional anti-cancer treatments.

INTRODUCTION

Lung cancer is a major health problem with an estimated 220,000 new cases per year in the United States. It is the leading

cause of cancer-related mortality and accounts for more deaths in men and women than the three next most common cancers combined: prostate/breast; colorectal; and pancreatic, which together attribute to 26%–28% of all cancer deaths (Siegel et al., 2014). Targeted therapies benefit only 15%–20% of non-small-cell lung cancer (NSCLC) patients harboring drug-sensitive mutations. Even in these patients, acquired resistance is a major impediment to a durable therapeutic response (Choi et al., 2010; Pao et al., 2005). Moreover, over 40% of NSCLC patients do not comprise identifiable driver mutations and thus lack actionable or druggable targets. Therefore, standard cytotoxic chemotherapy regimens remain the only therapeutic options for most NSCLC patients. However, these treatments eventually fail, resulting in acquired resistance and aggressive metastatic relapse within 5 years of diagnosis. Thus, molecular analysis of NSCLC is necessary to identify novel molecular targets that impact disease prognosis and the design of novel targeted therapies. In this context, more-recent studies have begun to focus on the tumor microenvironment (TME) as an unexplored target for drug discovery (Blumenschein, 2012).

TME is heterogeneous and includes reprogrammed or activated immune cells, cancer-associated fibroblasts (CAFs), and endothelial cells (Hanahan and Coussens, 2012). The concerted interactions between genetically altered cancer cells and intratumoral stromal cells regulate hallmarks of cancer, including angiogenesis, inflammation, immune suppression, invasion, epithelial-to-mesenchymal transition (EMT), and metastasis (Hanahan and Coussens, 2012). Notably, targeting intratumoral macrophages, in combination with standard cytotoxic chemotherapy, was effective in the treatment of breast cancer (DeNardo et al., 2011; Shree et al., 2011), and a similar approach was utilized in the treatment of glioblastoma (Pyontek et al., 2013).

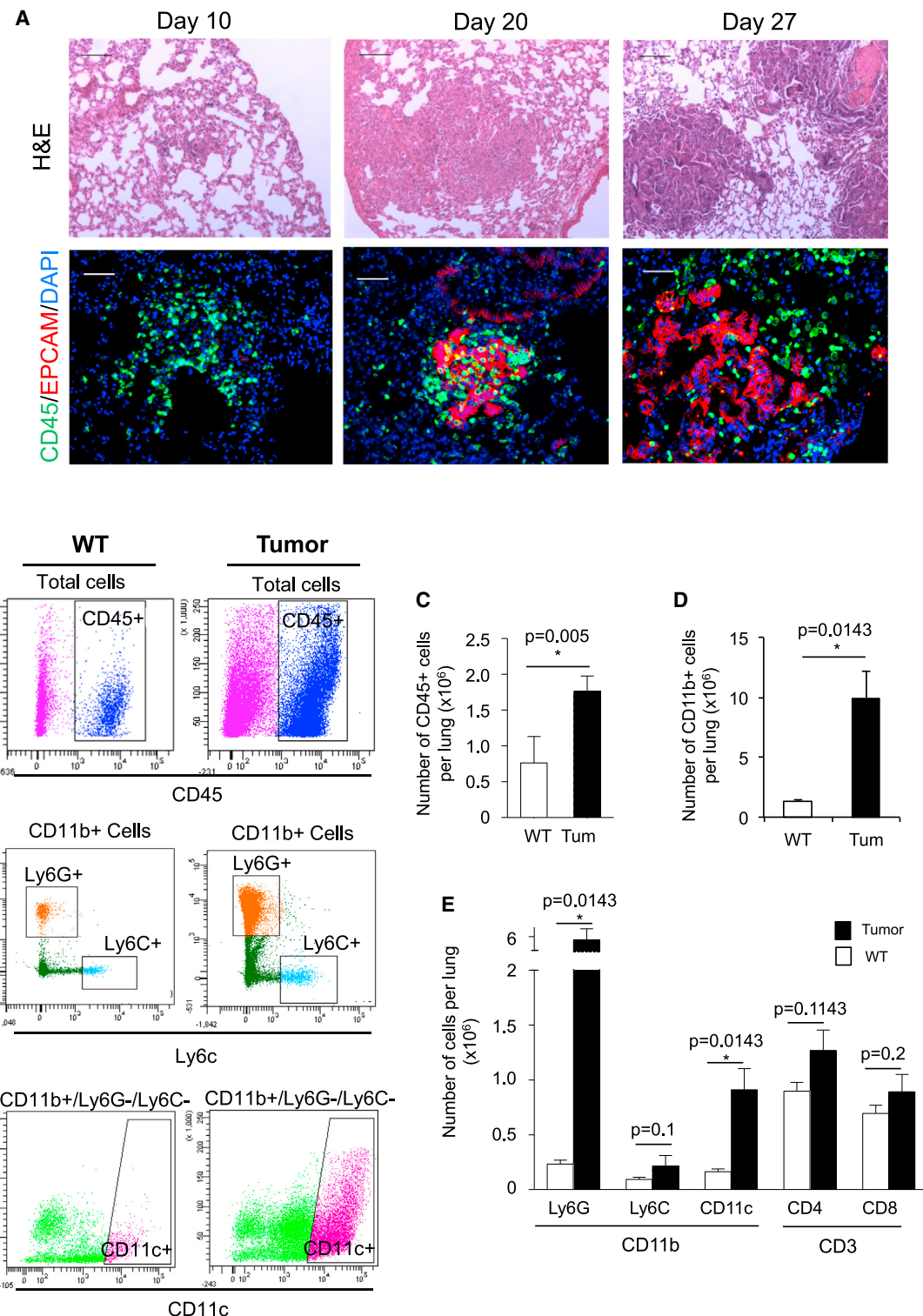


Figure 1. BM-Derived Cells Are Increased in Tumor-Bearing Lungs

(A) HGP1 orthotopic tumor-bearing lungs stained with H&E, scale bar 100 μ m (top), and with fluorescence-conjugated antibodies against CD45 and Epcam (bottom), scale bar 50 μ m.
(B) Flow cytometry scatterplots showing various subpopulation of cells in the lung from WT and HGP1-tumor-bearing mice. The parental cell population for each analysis is indicated on the top of each plot. Total number of lung cells was normalized with counting beads, and the same corresponding area of total lung cells from WT and tumor-bearing lungs is presented.

(legend continued on next page)

Although little is known about the precise role of stromal cells in NSCLC, a few studies have shown that the stromal elements confer prognostic value and may also contribute to resistance to targeted therapies in lung cancer. For example, in patients with stage I lung adenocarcinoma or squamous cell carcinoma, the presence of CAFs is considered a poor prognostic indicator, typically associated with nodal metastases and a higher risk of recurrence (Ito et al., 2012). Similarly, elevated recruitment of myeloid lineages including neutrophils and macrophages has been shown to confer prognostic value in NSCLC patients (Bel-llocq et al., 1998; Welsh et al., 2005). Furthermore, intratumoral stromal cells exhibit differential expression of genes compared with their non-tumor-associated counterparts. For example, intratumoral macrophages express increased cathepsin K, COX-2, MMP-9, PDGF-B, uPA, VEGFA, and HGF (Wang et al., 2011); neutrophils express neutrophil elastase (Houghton et al., 2010); and myeloid cells express PPAR γ (Li et al., 2011), suggesting that, in NSCLC, altered activation/reprogramming of stromal cells by the tumor epithelial cells contribute to tumor progression.

To characterize the stromal cell heterogeneity in lung cancer, we used an orthotopic model of NSCLC in syngeneic immunocompetent mice, which develops adenocarcinoma with histopathological similarities to human NSCLC. This model has enabled us to identify, quantify, and sort individual stromal and epithelial populations. We analyzed the transcriptomes of specific stromal and epithelial compartments sorted directly from tumor tissues and normal lungs and identified potential tumor-stroma paracrine and tumor autocrine crosstalk-signaling pathways using the newly developed computational crosstalk-signaling discovery model, Cell Cell Communication Explorer (CCCExplorer).

RESULTS

Establishment of an Orthotopic Model of Kras-Driven NSCLC

In the genetically engineered Kras-driven NSCLC mouse model, the *Kras*^{LSL-G12D/+;p53^{fl/fl} (KP) transgenic mouse develops lung adenocarcinoma following intratracheal instillation of lentiviral/adenoviral Cre recombinase (DuPage et al., 2009). Following Cre recombinase-mediated excision of the Kras oncogene stop element and the p53 gene, detectable adenocarcinomas are observed by 15–20 weeks. However, in this model, in addition to epithelial cells, stromal cells also have the potential to be infected by Viral-Cre. To determine the impact of virus infection on non-epithelial cells in the lungs, we generated the LSL- tdTomato; KP mouse. Administration of Viral-Cre showed that approximately 40% of tdTomato+ cells were CD45+ hematopoietic cells, suggesting that Viral-Cre infection has the ability to induce Kras activation and loss of p53 in the CD45+ cells (Figure S1A). Therefore, considering that CD45+ stromal cells are our main cell population of interest, and to avoid any}

potential alteration in the stroma mediated by Viral-Cre administration, we generated an orthotopic KP model in syngeneic immunocompetent mice. The orthotopic model maintains an intact host microenvironment during lung cancer progression.

A lung cancer cell line for developing the orthotopic model was derived from lung adenocarcinoma that was generated by intratracheal administration of Cre/luciferase-expressing lentivirus into a KP transgenic mouse (Figure S1B). The cells (HKP1) were delivered to the lungs via the tail vein, and lung tumor progression was monitored by *in vivo* bioluminescence imaging (BLI) (Figure S1C). HKP1-derived tumors were detectable in all animals as early as day 20, by both BLI and gross morphological analysis of lungs (Figure S1C). Notably, HKP1-derived adenocarcinomas were histologically comparable with the adenocarcinomas in KP transgenic mice (Figure S1D). Furthermore, the HKP1-derived tumors showed mixed histological subtypes including acinar and micropapillary adenocarcinomas, resembling phenotypes commonly observed in human adenocarcinoma (Solis et al., 2012; Figures S1E and S1F). The HKP1-derived orthotopic model was used to evaluate the contribution of the TME in tumor progression, by analyzing cellular composition and transcriptome of specific stromal and epithelial compartments that were sorted directly from the tumor parenchyma.

Lung Cancer Microenvironment Consists of Diverse Immune Cells

Bone-marrow-derived CD45+ hematopoietic cells contribute significantly to the TME in many cancer types (Hanahan and Coussens, 2012; Joyce and Pollard, 2009). Therefore, we investigated CD45+ hematopoietic cells in NSCLC by immunofluorescence microscopy and flow cytometry. An increase in the CD45+ population was observed in the lungs of HKP1-tumor-bearing mice (Figures 1A–1C), consistent with observations in spontaneous KP mice (Figure S2A) and in human lung adenocarcinoma (Figure S2D) by immunostaining. Flow cytometry analysis showed an increase in CD45+ cells in HKP1-tumor-bearing lungs compared to wild-type (WT) lungs (>2-fold more cells per lung; Figures 1B and 1C).

The heterogeneous CD45+ hematopoietic population includes cells of the myeloid lineage, subsets of T lymphocytes, and B cells (Ruffell et al., 2012). We analyzed these cellular subsets using specific cell-surface markers by flow cytometry (Figures S2E). CD11b+ cells representing the myeloid lineages were significantly ($p < 0.05$) increased in the TME (>7-fold; Figure 1D), whereas the CD4+ and CD8+ lymphocyte populations were not significantly elevated (Figure 1E). We further explored the CD11b+ myeloid lineages, as these cells have been implicated in promoting tumor growth by stimulating angiogenesis, mediating immune suppression, and promoting metastasis (Joyce and Pollard, 2009). Of the myeloid lineages, the CD11b+ Ly6G+ neutrophils were significantly ($p < 0.05$) increased in the TME (Figures 1B and 1E). We also identified CD11b+CD11c+ tumor-associated macrophages as significantly increased in

(C) Quantification of CD45+ cells in lungs from WT and HKP1-tumor-bearing mice by flow cytometry ($n = 3$).

(D) Quantification of CD11b+ cells in lungs from WT and HKP1-tumor-bearing mice by flow cytometry ($n = 3$).

(E) Quantification of subsets of CD11b+ and CD3+ cells in lungs from WT and HKP1-tumor-bearing mice by flow cytometry ($n = 3$).

Data are shown as mean \pm SEM. * $p < 0.05$ by Mann-Whitney U test.

the lung TME (Figures 1B and 1E). Consistent with published studies, the CD11b+ intratumoral macrophages lacked expression of Ly6G and Ly6C (Gr1 markers; Pyonteck et al., 2013) and expressed CD11c (Franklin et al., 2014; Figure 1B). Ki67 staining showed that a majority of CD11b+ cells (99.7%) in lung tumors were Ki67 negative (Figures S2F and S2G), suggesting that recruitment from the bone marrow compartments had resulted in elevated levels of myeloid lineage cells in the TME.

We next evaluated CD45+ stromal cell populations in spontaneous adenocarcinomas in KP transgenic mice. Consistent with the HKP1 tumors, KP tumors showed increased bone-marrow-derived CD45+ cells (Figures S2A and S2B) and an overall similar trend in the infiltration of various hematopoietic subsets (Figure S2C). Subtle differences were noted as well; for example, CD11b+Ly6G+ neutrophils were significantly ($p < 0.05$) increased in HKP1 tumors, but not in KP tumors (Figures 1E and S2C). This may reflect differences in the inflammatory state of the two models as neutrophils, the first responders to acute inflammation, are recruited extensively in rapidly growing orthotopic HKP1 tumors, compared with the slower-progressing spontaneous KP model. In addition, CD4+ T cells were not significantly increased in HKP1 tumors, whereas an increase in spontaneous KP tumors was noted. The T cells in early spontaneous KP tumors selectively eliminated antigen-expressing tumor cells, resulting in expansion of less-immunogenic tumors in an advanced stage (DuPage et al., 2011). Possibly, HKP1 cells, derived from advanced KP tumors, may have lower immunogenic potential compared to spontaneous KP tumors. Therefore, orthotopic tumors derived from HKP1 cells may harbor a diminished immune response as reflected by lower level of CD4+ cell recruitment.

The increased prevalence of specific bone-marrow-derived cells in the TME suggests that these stromal cells may contribute to NSCLC growth and that further molecular analysis could provide insights into their reprogrammed state.

Transcriptome Analysis Identified Differentially Expressed Genes from Individual Stromal and Epithelial Cell Populations in NSCLC

To determine the reprogrammed/activated state of intratumoral stromal cells, we focused on the CD11b+ myeloid lineages as they are significantly elevated and are known to contribute to tumor progression (Hanahan and Coussens, 2012). Moreover, these populations are amenable to FACS into discrete individual homogeneous subsets (monocytes, neutrophils, and macrophages), owing to distinct cell-surface markers and the availability of reliable antibodies (Figure S2E). Importantly, depletion of specific stromal subsets has been shown to impair tumor growth in various cancers, indicating their protumorigenic contribution in cancer (Pyonteck et al., 2013). We restricted our analysis to individual homogenous cellular compartments isolated directly from the tumor tissue to unravel cell-specific gene signatures, which could be missed when using heterogeneous populations in traditional bulk tumor profiling. Therefore, we did not include cell types such as fibroblasts, which are heterogeneous, and lack reliable reagents/methods to yield homogenous populations (Sugimoto et al., 2006). A schematic of the stromal and

epithelial cell populations used for transcriptomic analysis by RNA deep sequencing (RNA-seq) is shown in Figure 2A.

The stromal cell subsets and epithelial cells were sorted by flow cytometry from lung tissues freshly harvested from HKP1-tumor-bearing lungs and control WT lungs, using cell-type-specific surface markers (Figures 2B and S2E). WT resident macrophages were isolated based on their known surface markers CD11c+CD11b- (Guth et al., 2009). cDNA libraries were generated and sequenced using Illumina HiSeq2000 sequencers. RNA-seq was performed directly on sorted populations without subjecting them to in vitro culturing or RNA amplification to avoid any potential variances in transcript distribution.

Hierarchical clustering analysis on processed RNA-seq data showed discrete clustering of individual stromal subsets and epithelial cells from tumor-bearing and WT lungs (Figure S3). These results suggest that the RNA-seq data were sufficiently robust to identify tumor-specific differentially regulated genes in individual cell populations. We therefore used the LIMMA/Voom approach (Law et al., 2014; Smyth et al., 2002) to identify differentially expressed genes in tumor lungs compared to WT lungs. To visualize differences in gene expression in individual cellular subsets isolated from WT lungs and tumor lungs, we performed principal-component analysis (PCA) using all genes from each cell population. PCA showed that the WT and the tumor samples always segregated in two different areas of the 2D plots in the first dimension (PC1), indicating that the tumor signature is robust (Figure 2C). However, diversity captured by second dimension (PC2) was observed within WT samples of monocytes, neutrophils, and epithelial cells. Gene set enrichment analysis (GSEA) on genes that contribute to PC2 identified possible pathways that are significantly associated with the diversity of WT samples, such as immune response and Golgi transport pathways in neutrophils and epithelial cell population and cell-proliferation/cell-cycle-related pathways in monocytes (Table S1). Though the diversity in WT samples from monocytes, neutrophils, and epithelial cells does correlate with certain pathways, it is apparent that WT and tumor samples are always clearly separated along PC1, indicating that WT versus tumor signature dominates the data.

Next, the most differentially regulated genes in the intratumoral stromal subsets and tumor epithelial cells compared to their WT counterparts were determined using false discovery rate (FDR) $< 5\%$ (Figures 2D and 2E). Among them, we selected 43 genes for additional confirmation in an independent set of WT and tumor-bearing mice by qRT-PCR. The criteria for selection included fold changes (>2 -fold changes and FDR $< 5\%$) in specific intratumoral stromal cells and tumor epithelial cells. More than 80% of analyzed genes showed consistent expression patterns (fold changes and compartment specificity) between RNA-seq and qRT-PCR analysis (Figures 3A–3C and S4A–S4D). Analysis of the cells remaining after sorting the desired individual populations (Neg) confirmed that the candidate genes were differentially regulated only in the examined cellular compartments in tumor lungs (Figures S4C and S4D). Candidate genes including *Ccl7*, *Il23a*, and *Lgr4* were upregulated specifically in macrophages/monocytes, neutrophils, and epithelial

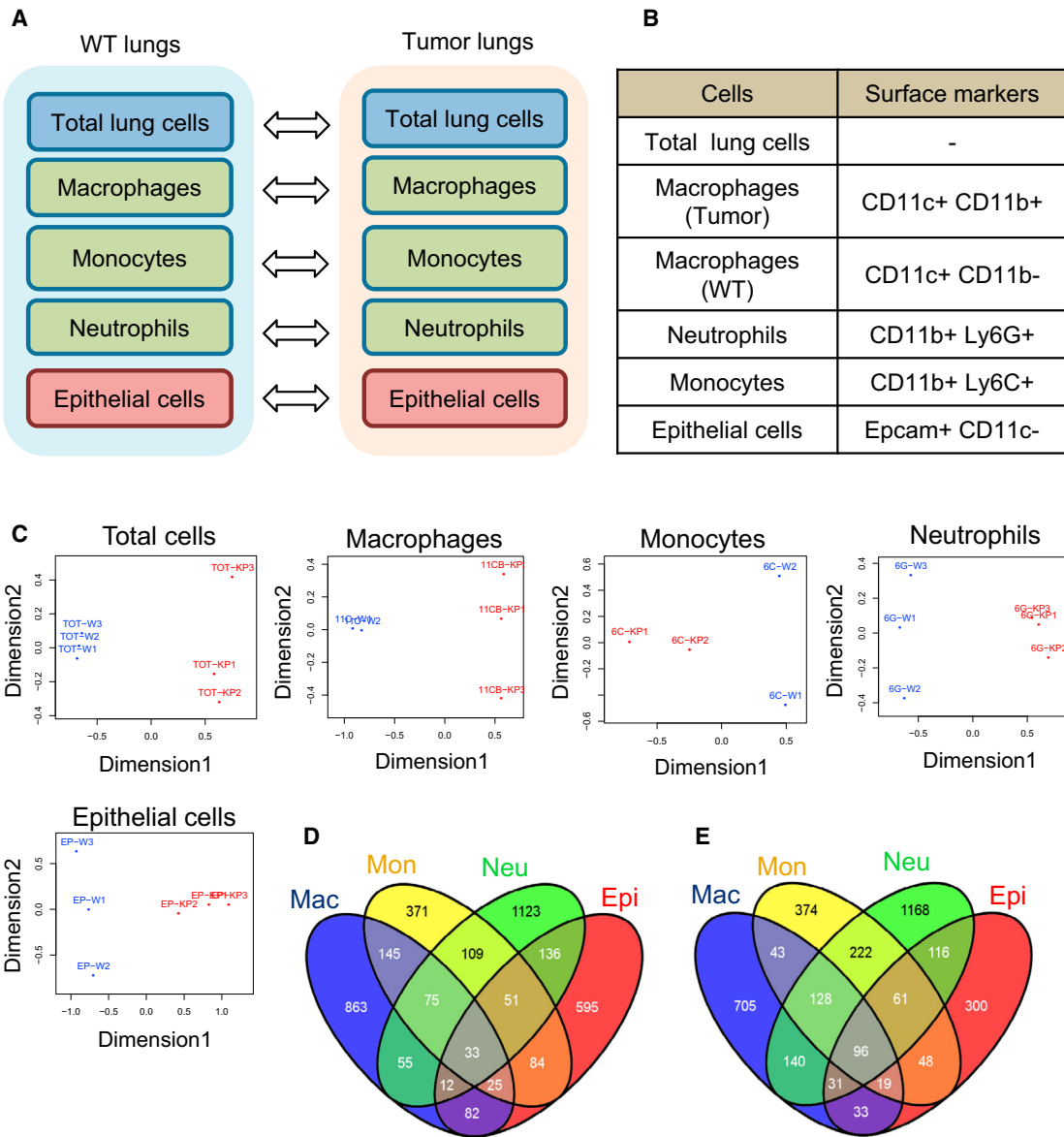


Figure 2. Individual Cellular Compartments from Tumor-Bearing Lungs Show Differential Gene Expression Profiles

- (A) Schema of RNA-seq analysis of individually isolated populations from WT and HKP1 tumor lungs.
- (B) Surface markers that were used for isolation of specific cell populations by FACS.
- (C) Principal component analysis (PCA) of RNA-seq data from individual cell populations and total lung cells. Red, tumor samples; blue, WT control samples.
- (D) Venn diagram showing upregulated genes from individual myeloid subsets and epithelial cells of tumor lungs compared to WT lungs. The cutoff is FPKM > 5, fold change > 2, and adjusted p value < 0.05. Epi, epithelial cells; Mac, macrophages; Mon, monocytes; Neu, neutrophils.
- (E) Venn diagram showing downregulated genes from individual myeloid subsets and epithelial cells of tumor lungs compared to WT lungs. The cutoff for upregulation is FPKM > 5, fold change > 2, and adjusted p value < 0.05. The cutoff for downregulation is FPKM > 5, fold change < -2, and adjusted p value < 0.05.

cell compartments, respectively, consistent with RNA-seq data (Figures 3A–3C). Furthermore, consistent with the RNA-seq and qRT-PCR data, immunofluorescence staining analysis of CCL7 and IL23A confirmed CD45+-cell-specific expression of candidate genes at the protein level (Figures 3D and 3E). Importantly, analysis of the spontaneous KP model showed that the candidate genes displayed significant correlation both in expression levels and compartment specificity (Figures S4E and S4F).

In the analysis above, we observed that, in a majority of cases, bulk tissue analysis (total lungs) failed to identify differentially regulated stromal genes (Figures 3A–3C, S4A, and S4B), highlighting our unique approach of utilizing individual sorted cell populations from heterogeneous tumor tissues and demonstrating why many of these genes with stromal-specific expression patterns had remained undiscovered in previous whole tumor profiling studies.

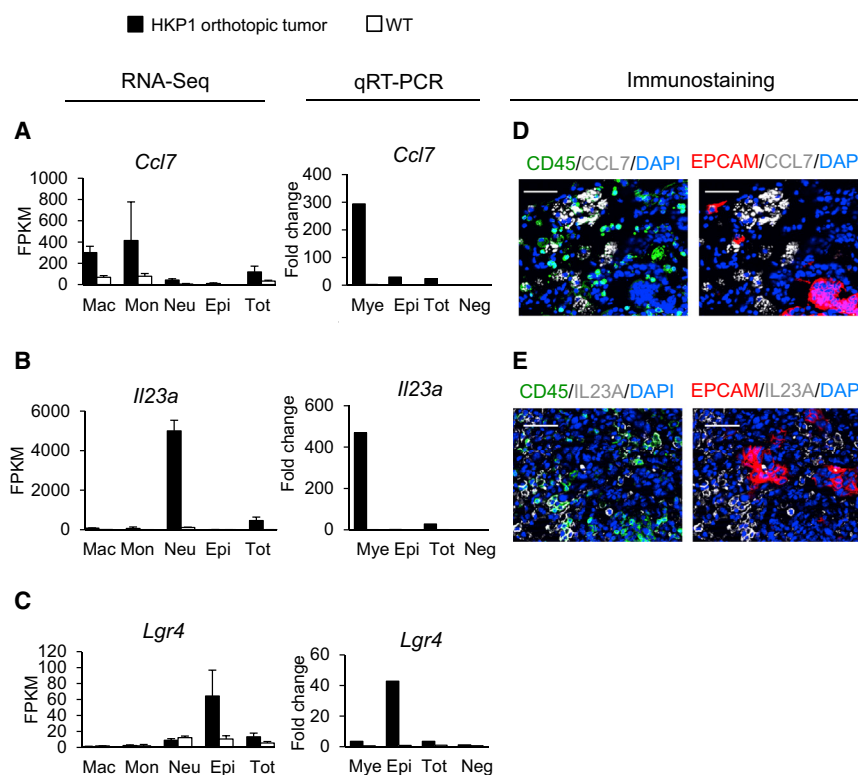


Figure 3. Representative RNA-Seq Analysis, qRT-PCR, and Immunostaining of Differentially Regulated Genes in Specific Individual Cellular Compartments

(A) Macrophage- and monocyte-specific differentially regulated genes.
 (B) Neutrophil-specific differentially regulated genes.
 (C) Epithelial-cell-specific differentially regulated genes.
 (D) Immunostaining of CCL7 with CD45 and Epcam antibodies in tumor-bearing lung; scale bar 50 μm.
 (E) Immunostaining of IL23A with CD45 and Epcam antibodies in tumor-bearing lung; scale bar 50 μm.
 Epi, Epcam+ CD11b–CD11c– cells; Mac, CD11c+CD11b+ cells (tumor), CD11c+CD11b– cells (WT); Mon, CD11b+Ly6C+ cells; Mye, mix of all CD11b+ cells and all CD11c+ cells; Neg, CD11b–CD11c– Epcam– cells; Neu, CD11b+Ly6G+ cells; Tot, total lung cells.
 Data are shown as mean ± SD.

Computational Analysis and Identification of Stroma-Tumor Paracrine Crosstalk and Tumor Autocrine Crosstalk in NSCLC

Tumor signaling is mediated by ligand-receptor interactions within both autocrine and paracrine pathways, which promote proliferation, survival, and migration in tumor cells (Wyckoff et al., 2004). Recent studies have begun to identify crosstalk pathways that have the potential to serve as attractive targets for anti-cancer therapy (DeNardo et al., 2011; Pyontek et al., 2013). However, so far only a limited number of crosstalk pathways have been identified in vivo, due to lack of concerted systematic and global discovery approaches. In this regard, our multi-cell RNA-seq data generated from tumor-bearing and WT lungs provides a unique opportunity to identify physiologically relevant stroma-tumor paracrine and tumor autocrine pathways.

Previous studies have reported network-based analysis for the identification of signaling networks in biological systems (Chuang et al., 2007; Komurov, 2012). However, there has been a lack of reliable computational tools for uncovering cross-talk pathways between multicellular-stromal components and tumor epithelial cells. Therefore, we developed a computational model, CCCExplorer, to uncover stroma-tumor crosstalk-signaling pathways as a directed and connected network from ligands-receptor interactions to transcriptional factors (TFs) and their target genes, as shown in Figure 4. In brief, upregulated ligands in tumor-associated stromal cells compared to WT counterparts and their corresponding receptors expressed in tumor epithelial cells were retrieved as potential crosstalk components. Activated downstream pathways of the receptors in tumor cells were identified by analyzing TFs, their upregulated target genes,

and signaling nodes in tumor epithelial cells. TFs were considered “activated” if their target genes were upregulated in the tumor epithelial cells compared to WT epithelial cells. Thus, signaling pathways comprised of upregulated ligands, expressed receptors, and activated downstream TFs were considered functional. Signaling nodes that connect receptors and TFs were derived from the signaling pathways information available in KEGG. In the crosstalk network, each signaling pathway was denoted by a directed graph, G, including nodes standing for the genes of ligands, receptors, TFs, and downstream target genes and edges for the interactions. The subgraph that was induced collectively by these components (upregulated ligands, expressed receptors, activated TFs, and upregulated target genes) was considered as an activated signaling branch. Each pathway branch deemed significant (Fisher’s test; $p < 0.05$) was combined to generate the crosstalk network. We simplified the combined network by linking receptors directly to the TFs and added the upregulated targets of the TFs. This model was applied to the RNA-seq data set, and three paracrine and one autocrine network were generated.

This modeling required comprehensive ligand-receptor network information. The known ligand-receptor information was obtained from databases including KEGG (Ogata et al., 1999) and DLRP (Graeber and Eisenberg, 2001). However, these data sets are incomplete; thus, we derived the subcellular localizations of all available proteins in the HPRD database (<http://www.hprd.org>) and isolated protein sets with subcellular localizations in “extracellular” and “secreted” to identify additional ligands to complement the KEGG and DLRP database (Komurov, 2012). Cognate receptors of these ligands were identified by analyzing protein interactions from the STRING database (Szklarczyk et al., 2011). The selected ligand-receptor pairs were evaluated manually to confirm interactions using published literature. This allowed us to establish a ligand-receptor

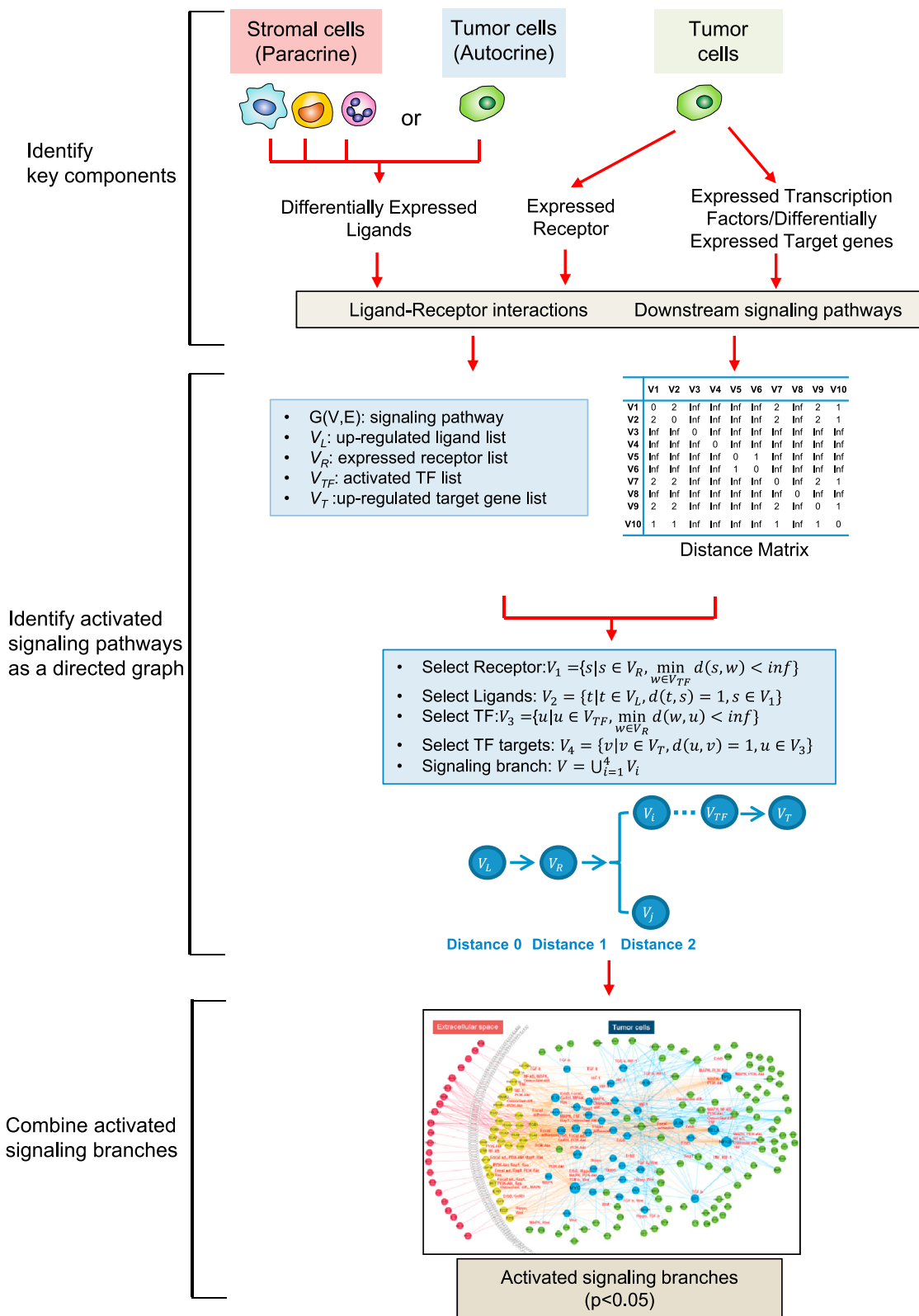


Figure 4. Computational Analysis of Paracrine/Autocrine Crosstalk
Flow chart depicting CCCExplorer model. See also Experimental Procedures.

interaction database that included 436 ligands, 325 receptors, and 1,433 ligand-receptor interactions for crosstalk analysis.

We first selected differentially regulated ligands in the intratumoral stromal cells and tumor epithelial cells compared to WT counterparts, using a set of selection criteria based on FPKM > 2, fold change > 1.5, and adjusted p value < 0.1 (Table S2). Similarly, we selected cognate receptors on tumor epithelial cells with FPKM values > 2 (Table S2). Using these criteria, we identified upregulated ligands from individual intratumoral cellular compartments (61 in macrophages, 32 in monocytes, 25 in neutrophils, and 62 in tumor cells; Table S2) and 149 genes encoding receptors expressed in tumor epithelial cells (Table S2). Most of the ligands passing our threshold have a corresponding adj. p < 0.05. TFs and their target gene information were obtained from KEGG and TRED (<https://cb.utdallas.edu/cgi-bin/TRED/tred.cgi?process=home>). Expressed TFs in tumor cells were screened using FPKM > 2, and their target genes that were upregulated were identified using the same criteria as selecting ligands (Table S2). FPKM values of >1 have been widely used to identify expressed transcripts in RNA-seq analysis (Hart et al., 2013). The FPKM > 2 threshold in CCCExplorer modeling reliably identifies TFs, which are known to be expressed at low levels and are critical in the determination of crosstalk networks. In addition to these FPKM and fold-change thresholds, additional stringent parameters in the form of p value cutoffs also enhance significance to select differentially expressed genes (adjusted p value < 0.1, from three independent RNA samples) in tumor samples compared to WT samples and crosstalk-signaling pathways (p value < 0.05; ligand-receptor-TFs-target genes). Mouse genes were converted to human orthologous using the mapping provided by Mouse Genome Informatics database.

From the CCCExplorer analysis, we identified individual stromal-cell-derived, differentially regulated ligands that contribute to activation of downstream signaling pathways in tumor epithelial cells. Heatmap analysis of those ligands demonstrated cell-type-specific clustering and upregulated expression in tumor samples compared to WT samples (Figure 5). FPKM, fold change, and adj. p values of upregulated ligands from macrophage-tumor crosstalk network are shown (Figure 5). Consistently, heatmap of all genes also demonstrated cell-type-specific gene expression (Figure S5).

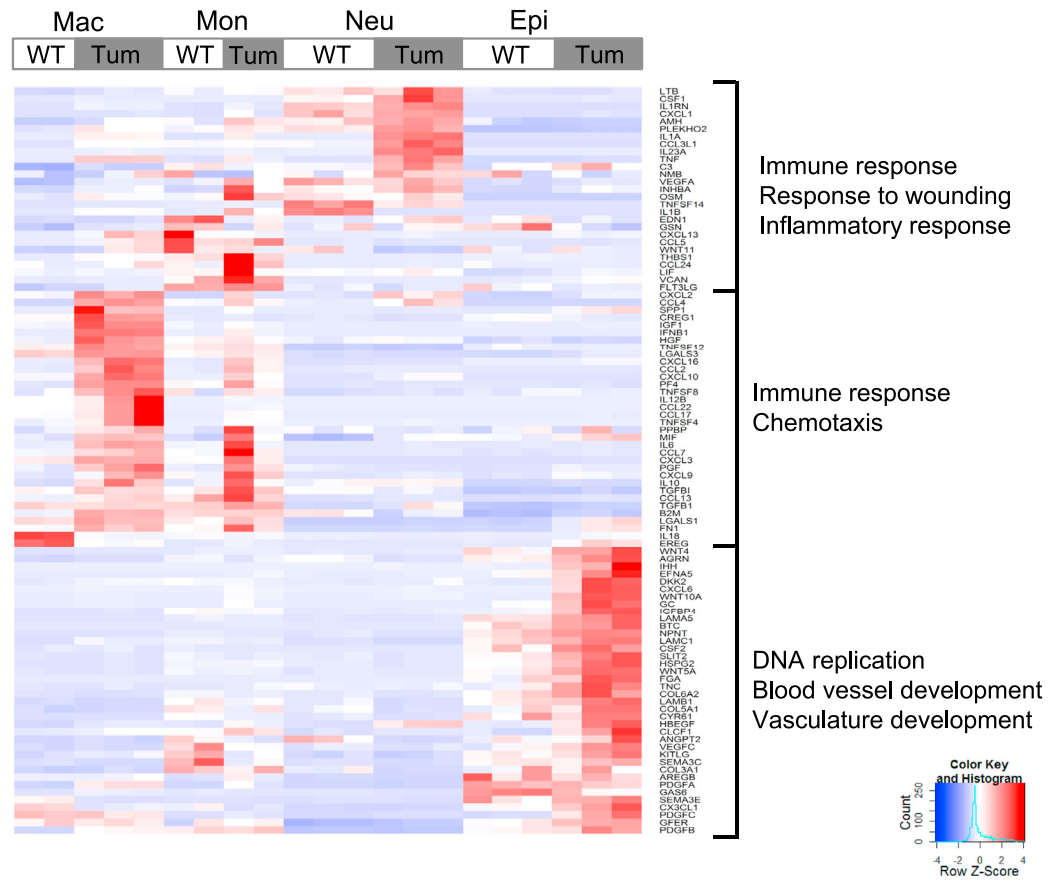
CCCExplorer analysis identified pathways that are activated by paracrine/autocrine crosstalk specifically and included both previously described and relatively novel signaling pathways in NSCLC. Tumor-promoting pathways including MAPK, PI3K-Akt, NF-kappa B, ErbB, Ras, TGF- β , and TNF signaling pathways were activated by all of the stroma-tumor paracrine and tumor autocrine crosstalk (Figures 6, S6, and S7). Importantly, we identified potentially novel paracrine crosstalk pathways including IL6-IL6R between macrophages and tumor cells in NSCLC. In the CCCExplorer analysis, the IL6-IL6R ligand-receptor interaction was predicted to uniquely activate HIF-1 signaling. IL6, a potent activator of STAT3, has been shown to be secreted by tumor cells in various cancer types (Schafer and Brugge, 2007). In NSCLC, whereas a tumor autocrine role of IL6 has been implicated in carcinogenesis (Gao et al., 2007), the paracrine crosstalk between stromal IL6 and tumor IL6R has not been reported.

Similarly, the CCCExplorer analysis identified novel paracrine activation of Wnt-signaling pathway. Macrophages expressed WNT11 and tumor cells expressed the FZD7 receptor, indicative of a paracrine crosstalk pathway. Though many studies showed the tumor-promoting role of autocrine Wnt-signaling pathways (Anastas and Moon, 2013), paracrine contribution on activation of Wnt signaling in lung cancer has not been reported.

The macrophage-tumor (Mac-Tum) crosstalk included 22 macrophage-derived differentially regulated ligands and the presence of 31 cognate receptors on tumor epithelial cells (Figure 6; Table S3). The interactions between these ligands and receptors are predicted to induce activation of 39 TFs, leading to the induction of 14 significant (p < 0.05) signaling pathways in NSCLC (Figure 6; Table S3). In the Mac-Tum crosstalk analysis, we identified unique paracrine crosstalks including the HGF-MET, THBS1-integrin, TNFSF14-LTBR, VEGFA-FLT1, and WNT11-FZD5/7 between macrophages and tumor epithelial cells (Figure 6). Importantly, we were able to discern potentially novel mediators of the activated signaling pathways including TNFSF14-TNFRSF1A, FN1-integrins, SPP1-integrins, IFNB1-IFNAR1/2, IL6-IL6R, and LTB-LTBR in lung cancer (Table S3). Mac-Tum crosstalk also showed significant induction of the Wnt-signaling pathway (Wnt11-FZD7 axis), whose role has remained unclear in NSCLC *in vivo*.

Monocytes-tumor (Mon-Tum) crosstalk included 11 monocyte-derived ligands and 16 cognate receptors on tumor cells. These ligand-receptor pairs are predicted to induce ten signaling pathways (p < 0.05) through 31 TFs (Figure S6A; Table S4). Whereas many of these pathways were also observed in the Mac-Tum analysis above, specific crosstalk pathways including the AREG-EGFR signaling were also identified. The AREG-EGFR axis activates ErbB signaling (Table S4) and has been reported in diverse cancer types including breast, colorectal, brain, and liver (Katoh and Katoh, 2006). In lung cancer cells, elevated levels of AREG has been shown to inhibit apoptosis (Hurbin et al., 2002) and leads to resistance to the EGFR inhibitor gefitinib (Busser et al., 2010). Therefore, in our analysis, the identification of the AREG-EGFR axis *in vivo* suggests a potential tumor-promoting role in NSCLC.

Neutrophil-tumor (Neu-Tum) crosstalk included eight neutrophil-derived ligands and 17 cognate receptors on tumor epithelial cells. The interactions between these ligands and receptors are predicted to induce 33 TFs, leading to the activation of 11 significant (p < 0.05) signaling pathways in NSCLC (Figure S6B; Table S4). Distinctively, Neu-Tum crosstalk revealed the TGFB1-TGFBRII interaction, which was not observed in other stroma-tumor crosstalk (Figure S6B). The dual role of TGF- β 1 in cancer is reported in many cancer cells. The anti-proliferative and apoptotic tumor-suppressive activity of the TGF- β 1-TGF- β type II receptor interaction is compromised in many cancer cells. In addition to compromised tumor-suppressive signaling arm, TGF- β promotes tumor growth, invasion, and metastasis. Further, TGF- β contributes to tumor growth by suppressing anti-tumor immune and inflammatory response (Massagué, 2008). In lung cancer, elevation of TGF- β 1 has been observed in tumor and blood of lung cancer patients (Barthelemy-Brichant et al., 2002; Kim et al., 1999). Furthermore, expression of TGF- β type II receptor is commonly observed to be reduced in lung



Ligands	Mac_WT FPKM	Mac_Tum FPKM	Fold change	Adj. p value	Ligands	Mac_WT FPKM	Mac_Tum FPKM	Fold change	Adj. p value
IFNB1	0	267.42	Inf	<0.05	TNFSF14	0.628379	4.33775	6.903079	<0.05
THBS1	1.9728	210.264	106.582	<0.05	TNF	256.062	1445.51	5.645143	<0.05
IL1B	42.9315	1326.23	30.89176	<0.05	HBEGF	1.59394	8.92968	5.602303	<0.05
VEGFA	7.99474	167.936	21.00586	<0.05	IL1A	110.252	600.329	5.445068	<0.05
SPP1	333.622	6810.59	20.41404	<0.05	HGF	3.53725	16.4049	4.637766	<0.05
INHBA	0.64984	9.97331	15.34737	<0.05	LTB	3.2082	10.3578	3.228536	<0.05
IL6	5.64875	85.1163	15.06815	<0.05	LAMC1	1.94792	5.41678	2.7808	<0.05
CSF1	1.76133	25.9923	14.75723	<0.05	FN1	152.726	408.997	2.67797	<0.05
IGF1	4.99084	59.4332	11.9085	<0.05	OSM	136.577	334.441	2.448741	<0.05
PGF	1.1438	11.3651	9.936378	<0.05	COL3A1	1.56164	2.74464	1.757542	<0.05
WNT11	0.549302	4.74061	8.630236	<0.05	COL27A1	1.9277	3.10939	1.613007	<0.05

Figure 5. Heatmap Depicting Differentially Regulated Ligands across Cell Populations Derived from Lungs from WT and HKP1-Tumor-Bearing Mice

Heatmap was generated using gplots R package (Warnes et al., 2014) from selected upregulated ligands (FPKM > 2, fold change > 1.5, and adj. p < 0.1) of each cell type. The enriched functions (GO terms) of specifically upregulated genes were analyzed using DAVID (<http://david.abcc.ncifcrf.gov/>). A table shows FPKM and fold change of the ligands from macrophage-tumor crosstalk network.

cancer epithelial cells (Anumanthan et al., 2005; Kim et al., 1999). However, the function of TGF- β in lung cancer progression is controversial. Dysregulation of TGF- β signaling was identified as an important mediator of lung cancer invasion (Toonkel et al., 2010). In contrast, TGFBRII siRNA treatment suppressed tumor cell proliferation and invasion and increased apoptosis of the A549 lung cancer cell line in vitro (Xu et al., 2011) and

TGF- β 1 promotes lung cancer growth indirectly by polarization of macrophages via IRAK-M (Standiford et al., 2011).

In the HKP1 lung cancer model, TGF- β type II receptor expression is not significantly reduced (adj. p > 0.05) in tumor cells. Thus, extensive mutation analysis on TGF- β type II receptor and cytostatic genes including p15INK4b and c-MYC may provide important insights into the contribution of TGF- β -signaling

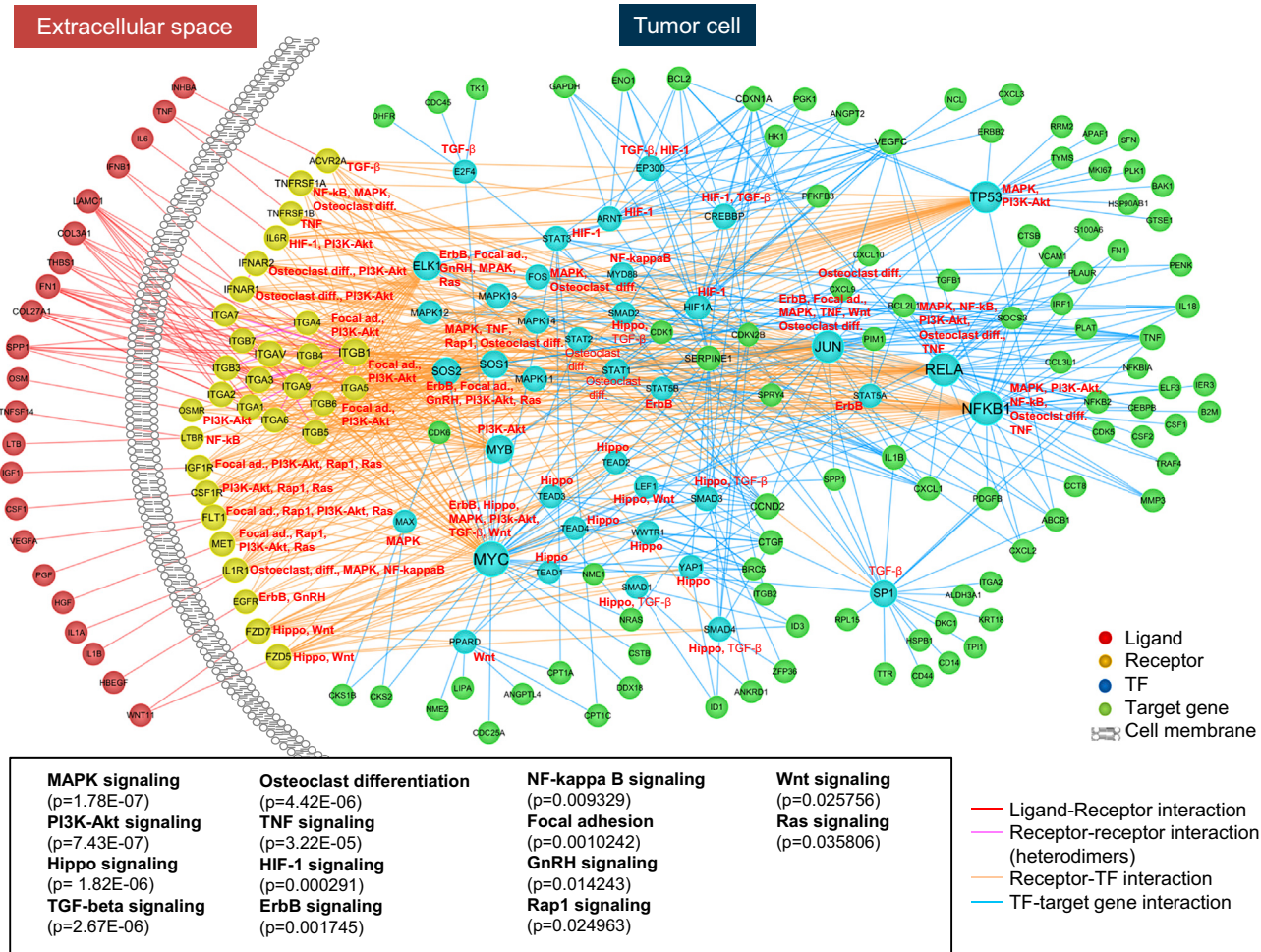


Figure 6. Paracrine Crosstalk Network between Macrophages and Tumor Cells

Macrophage-derived ligands in extracellular space, cognate receptors, transcription factors, and downstream target genes in the tumor cells generate networks of activated signal transduction pathways. The signaling pathways that are significantly activated by these interactions ($p < 0.05$ by Fisher test) are depicted in a box (see also Table S4).

pathway in NSCLC, as observed in subsets of breast cancer (Gomis et al., 2006).

In addition to stroma-tumor paracrine crosstalk analysis, we evaluated tumor autocrine crosstalk signaling. This included 22 tumor-derived ligands and 29 cognate receptors on tumor cells. The interactions between these ligands and receptors are predicted to induce 33 TFs, leading to the activation of 12 tumor-signaling pathways (Figure S7; Table S5). The CCCExplorer analysis identified unique crosstalks in tumor autocrine signaling of lung cancer, such as BTC-EGFR, EFNA5-EPHA2, EREG-EGFR, WNT10A-FZD5/7, WNT4-FZD5/7, and WNT5A-FZD1/2/5/7. In addition, distinct upregulation of diverse extracellular matrix (ECM) components such as fibronectin, tenascin C, collagens, and laminin variants has the potential to regulate tumor cell behavior through their unique physical, biochemical, and biomechanical properties in lung cancer. Furthermore, ECM interactions with receptors on tumor cells induce signal transduction in tumor cells (Kessenbrock et al., 2010). Previous studies have shown that interaction of

ECM proteins and β 1-integrin protects cancer cells against apoptosis in small cell lung cancer (Sethi et al., 1999). Although little is known in NSCLC, our analysis suggests that the ECM-integrin interactions may contribute to focal adhesion and PI3K-Akt-signaling pathway activation in NSCLC (Table S5).

Individual myeloid cells displayed common ligand-receptor interactions, involving IL1A, TNF, INHBA, and HB-EGF, suggesting that cells were reprogrammed in a similar way in the TME. Whereas paracrine crosstalk pathways between individual stromal cells and tumor epithelial cells revealed similarities with many common ligand-receptor interactions, tumor autocrine crosstalk pathways displayed unique pathways mediated by BTC-EGFR, EREG-EGFR, collagen-integrins, TNC-integrins, and laminins-integrins, diverse WNT ligands (WNT4, WNT5A, and WNT10A).

Interestingly, irrespective of the cell type, we also observed global ligand-receptor interactions including the INHBA-ACVR2A axis, indicating that multiple cell populations are

involved in activation of a single pathway. Increased INHBA expression has been shown to promote tumor cell proliferation in lung adenocarcinoma (Seder et al., 2009), and its upregulation is associated with poor outcome in lung adenocarcinoma and gastric cancer (Seder et al., 2009); however, its role in lung cancer is not fully understood. The complexity of the TME was also observed in the form of expression of multiple variants of ligands and receptors. For example, we observed multiple variant WNT ligands from macrophages (WNT11) and tumor cells (WNT4, WNT5A, and WNT10) and multiple FZD receptor (FZD5, FZD7, and FZD8) expression on tumor cells, indicating combinatorial ligand-receptor interactions and a diverse level of Wnt or Hippo signaling pathway regulation.

Identification of activated downstream signaling pathways suggested that the identified ligand-receptor crosstalk has the potential to trigger physiological and functional changes via signal transduction pathways in tumor cells. Importantly, a number of ligand-receptor interactions (both paracrine and autocrine) that do not have annotated downstream signaling pathways were also identified (Tables S3, S4, and S5). Future studies will be necessary not only to determine their roles in carcinogenesis but also to evaluate their potential as novel diagnostic, prognostic, or therapeutic targets for lung cancer.

Experimental Validation of CCCExplorer-Predicted IL6-IL6R Paracrine Crosstalk Pathway between Macrophages and Tumor Epithelial Cells

Among the potential crosstalk pathways predicted by the CCCExplorer analysis, we selected the IL6-IL6R macrophage-tumor paracrine crosstalk pathway for experimental validation. In HKP1 tumors, IL6 expression was specifically increased in the macrophages and monocytes compared to WT counterparts (Figure 7A). Noticeably, the IL6 receptor was expressed in HKP1 tumor epithelial cells (Figure 7B). Previous studies have shown that IL6 is a potent activator of the JAK/STAT3 pathway (Zhong et al., 1994), and both autocrine and paracrine IL6/STAT3 signaling has been shown to promote breast cancer progression (Chang et al., 2013). We chose the IL6-IL6R-STAT3 paracrine pathway because, in lung cancer, the autocrine role of IL6 in inducing STAT3 has been demonstrated (Gao et al., 2007); however, the paracrine crosstalk between stromal IL6 and tumor IL6R has not been reported. Therefore, to test the paracrine-signaling pathway, we established an in vitro system comprised of macrophages and HKP1 tumor cells. Macrophages were differentiated from freshly harvested murine bone marrow cells as described (Weischenfeldt and Porse, 2008), with an efficiency of >90% as determined by expression of CD11b, CD68, and F4/80 (Figure 7C).

To emulate the paracrine interaction in the TME in vitro, we used an experimental approach depicted in Figure 7D. Using this approach, we observed that HKP1 tumor-conditioned media (T-CM), which did not contain IL6, was able to stimulate IL6 production in WT macrophages, but not in $\text{IL6}^{-/-}$ macrophages, as determined in MacT-CM (Figure 7E). Strikingly, MacT-CM activated STAT3 significantly (>10-fold, compared to Mac-CM) in HKP1 tumor cells as determined by elevated phospho-STAT3 levels (Figure 7F). Notably, MacT-CM derived

from $\text{IL6}^{-/-}$ macrophages failed to activate p-STAT3 significantly, suggesting that IL6 in the macrophage supernatant mainly contributes to STAT3 activation in tumor cells. Next, we determined the paracrine role of IL6 in conferring protumorigenic properties on tumor cells. Treatment of HKP1 cells with recombinant IL6 increased migration and impaired apoptosis, indicative of a tumor-promoting function of IL6-IL6R interaction (Figures 7G and 7H).

Together, these findings not only validate the IL6-IL6R-STAT3 paracrine crosstalk pathway predicted by the CCCExplorer analysis but also suggest the therapeutic potential of targeting this pathway in NSCLC.

DISCUSSION

In previous studies, a limited number of tumor-stroma crosstalk pathways have been identified. Importantly, these pathways have been shown to contribute significantly to carcinogenesis, warranting a more systematic genome-wide analysis to unravel additional pathways. In this context, genomic analysis of limited stromal cells in breast cancer identified cell-specific targets (Allinen et al., 2004). However, in this study, comprehensive crosstalk pathways analysis was not performed. Other studies have relied on in vitro co-culture analysis, and the in vivo utility of the identified pathways has been limited.

Here, a systematic analysis of individual stromal and epithelial compartments in NSCLC, together with a predictive modeling, has revealed known and relatively novel key tumor-stromal paracrine and tumor autocrine crosstalk pathways in the lung cancer microenvironment, with information of specific producers of ligands. The experimental design employed in this study is innovative and is the first to use genome-wide RNA-seq analysis of purified individual stromal and epithelial cell compartments directly from freshly procured tissues. The design allowed quantitative analysis of differentially regulated genes in specific cell populations of interest, particularly stromal cells, which are often missed in traditional whole bulk tumor tissue profiling. Another unique feature is the development of the CCCExplorer model to computationally integrate multicellular transcriptome- and interactome-signaling data and to incorporate existing ligand-receptor interactions to discover and score the inter-cellular crosstalk-signaling pathways.

Whereas we have identified potential crosstalk pathways in NSCLC, a reasonably complete, graphic depiction of the network of microenvironmental signaling interactions is still far beyond our reach, as many signaling molecules and pathways remain unclear. Furthermore, the computational analysis of paracrine and autocrine pathways relied solely on transcriptome profiles of individual cellular stromal subsets and tumor epithelial cells from NSCLC. Whereas the transcriptomic profiles provided quantitative changes in gene expression levels of ligands, receptors, and components of the downstream signaling pathways such as TFs and their target genes, limitations associated with the absence of protein data impose significant challenges in the identification of many activated pathways. Thus, future studies should incorporate analysis of phosphorylated proteins, which are more-robust indicators of downstream signaling.

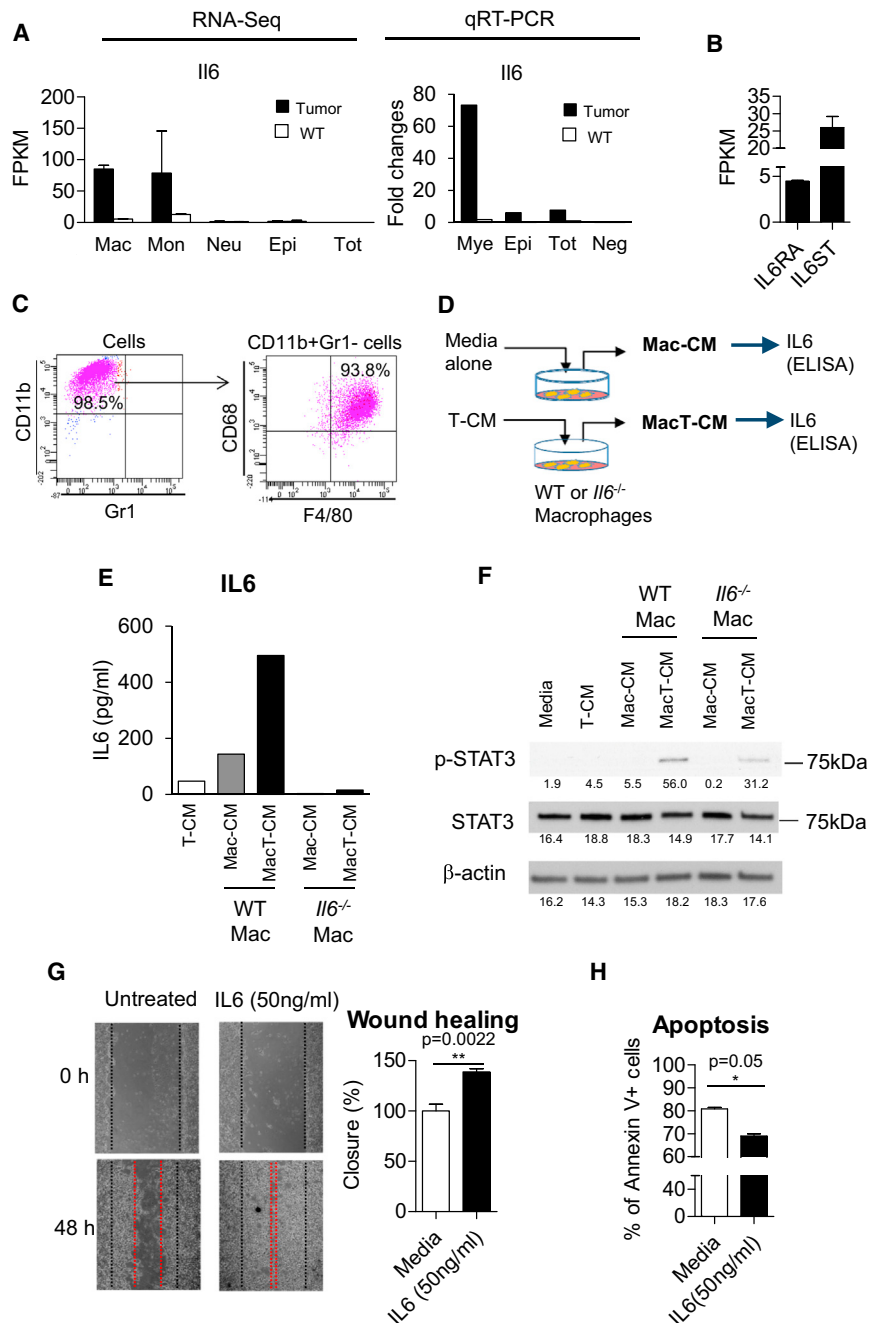


Figure 7. Experimental Validation of IL6-IL6R Paracrine Crosstalk between Macrophages and Tumor Epithelial Cells

(A) RNA-seq and qRT-PCR analysis of *Il6* expression from individually isolated populations from WT and HKP1 tumor lungs. Data are shown as mean \pm SD.

(B) RNA-seq analysis of IL6 receptor genes in tumor epithelial cells. Data are shown as mean \pm SD.

(C) Flow cytometry analysis of macrophages differentiated from bone marrow cells, using cell surface markers CD11b, Gr1, CD68, and F4/80. The parental cell population for each analysis is indicated on the top of each plot.

(D) Schema depicting treatment of macrophages with media alone or tumor-conditioned medium (T-CM) to generate macrophage-conditioned medium, Mac-CM and MacT-CM, respectively.

(E) ELISA of IL6 from WT or $\text{IL6}^{-/-}$ macrophage CM generated by the schema described in (D). Each sample was pooled from more than three wells.

(F) Western blot of p-STAT3 and STAT3 in HKP1 tumor cells following treatment with conditioned media (Mac-CM and MacT-CM) from WT macrophages and $\text{IL6}^{-/-}$ macrophages. Bands were quantitated, and values are presented below each blot.

(G) HKP1 cell wound healing assay with IL6 treatment ($n = 3$). Data are shown as mean \pm SEM. * $p < 0.05$ by Mann-Whitney U test.

(H) Apoptosis assay with annexin V in HKP1 tumor cells following recombinant IL6 treatment ($n = 3$). Data are shown as mean \pm SEM. * $p < 0.05$ by Mann-Whitney U test.

ease and may lead to the development of potential novel stromal therapeutic targets against NSCLC, particularly Kras-driven adenocarcinoma, either alone or in combination with conventional treatments that target cancer cells.

EXPERIMENTAL PROCEDURES

For further details, please see the [Supplemental Experimental Procedures](#).

All animal work was conducted in accordance with a protocol approved by the Institutional Animal Care and Use Committee. Human lung adenocarcinoma was obtained from New York Presbyterian Hospital/Weill Cornell Medical College in accordance with a protocol approved by the IRB.

RNA-Seq Analyses

RNA-seq reads were analyzed using FastQC to detect potential problems. Then, short reads were aligned to the mm9 reference genome using TopHat with default parameters. FPKMs (fragments per kilobase per million mapped reads) (Mortazavi et al., 2008) were determined for all RefSeq genes using CuffLinks. Read counts were obtained using HTseq (Anders et al., 2014).

Differential expression analysis was performed using the LIMMA/Voom approach. We used PCA to determine how individual samples relate to each

Despite these limitations, our approach has identified known and novel paracrine crosstalk pathways between individual myeloid and tumor cells and tumor cell autocrine pathways. The experimental validation of IL6-IL6R paracrine crosstalk pathway between macrophages and tumor cells confirmed that other paracrine crosstalk pathways discovered by CCCExplorer analysis may have also functional significance. Therefore, rapid experimental validation of the CCCExplorer-predicted crosstalk pathways constitutes an essential next step to consider mechanistic explorations *in vivo*. Exploring the mechanistic basis of these pathways is likely to confer insights into the biology of the dis-

other based on all gene expression profiles. Differentially regulated genes were further analyzed for overlap and visualized using Venny (Oliveros, 2007).

Development of the CCCExplorer Model

The workflow for modeling and discovering multi-crosstalk in CCCExplorer is given below.

Algorithms to find activated pathway branches:

Find all upregulated ligands in stromal cells, denoted by L , and all expressed receptors in tumor cells, denoted by R . All LR interactions with ligands in L and receptors in R are selected as potential crosstalks between stromal and tumor cells.

Find all upregulated genes in tumor cells, denoted by T_{up} . For each TF, let L_{TF} denote its targets list. Let L_{all} denote all annotated gene lists in the data-matched human orthologous. Fisher test is applied where $a = |T_{up} \cap L_{TF}|$, $b = |T_{up}| - a$, $c = |L_{TF}| - a$, $d = |L_{all}| - (a + b + c)$ and probability P is calculated by

$$P = \frac{\binom{a+b}{a} \binom{c+d}{c}}{\binom{a+b+c+d}{a+c}}$$

$\binom{n}{k}$ is the binomial coefficient. Then, the p value is calculated using stats R package. Those with $p < 0.05$ are considered as activated TFs, denoted by T_{TF} .

For each KEGG pathway, remove the ligands that are not in L and receptors that are not in R . For all other genes, create a directed network $G(V, E)$, where V stands for the gene sets in the pathway and E stands for the interactions between them. Calculate the distance matrix $D = (d_{ij})$, where d_{ij} is the distance from V_i to V_j , i.e., the length of shortest pathway from V_i to V_j . For $V_i \in L$, find all nodes that are reachable from V_i , denoted by N_{V_i} , where $d_{ij} < \text{Inf}$ for every $V_j \in N_{V_i}$. Let $N_L = \sum_{V_i \in L} N_{V_i}$. For $V_k \in T_{TF}$, find all nodes that can reach V_k , denoted by N_{V_k} , where $d_{ik} < \text{Inf}$ for every $V_i \in N_{V_k}$. Let $N_{TF} = \sum_{V_k \in T_{TF}} N_{V_k}$. Finally, the subgraph induced by $V_{link} = N_L \cap N_{TF}$ is considered as activated pathway branch, denoted by $H = G[V_{link}]$.

The significance of downstream genes in each activated signaling branch H was evaluated using Fisher test similar to the one used by testing TFs. All ligands and receptors were excluded because we only focused on the downstream signaling of receptors. Activated TFs were considered upregulated regardless of their expression values in tumor cells. Those pathway branches with $p < 0.05$ were selected as significant activated pathway branches, denoted by H_{sig} . We then revised H_{sig} by linking the ligands directly to the activated TFs and adding in the activated target genes of these TFs. The cell communication network between each stromal and tumor cells is then the combination of H_{sig} , i.e., $\bigcup H_{sig}$.

The codes are available at <http://209.160.41.231/u54/CCCEexplorer/>.

Paracrine/Autocrine Crosstalk Computational Analysis

For CCCEexplorer analysis, RNA-seq reads were analyzed using the computational pipeline from the S.T.C.W. lab at Houston Methodist hospital for crosstalk analysis. Briefly, fragment reads were mapped to UCSC mouse genome (mm10/GRCm38) using Tophat2. Raw counts for each gene were obtained by Cufflinks and then converted to FPKMs and scaled via the median of the genomic means for each gene across all libraries as described (Anders and Huber, 2010). Adjusted p values for each gene were obtained by cuffdiff 2. Activated pathway branches were found using the CCCEexplorer model on RNA-seq data from isolated myeloid and epithelial cells. The significance of each pathway branch that was activated in the crosstalk was evaluated using the Fisher test.

In Vitro Macrophage Differentiation Experiment

To obtain macrophages, total bone marrow was harvested from C57BL/6J WT mouse (Jax 00064) and $Il6^{-/-}$ mouse (Jax 2650) and cultured for 7 days in DMEM supplemented with 10% FBS, L-glutamine, penicillin/streptomycin, and 20% of L929 cell-conditioned media enriched for CSF1 for macrophage differentiation. L929 cell-conditioned media was prepared from confluent L929 in DMEM-supplemented 10% FBS, L-glutamine, and penicillin/streptomycin. To collect macrophage-conditioned media for tumor cell treatment, 1

million macrophages were seeded in a well of 6-well plates and treated either with serum-free HKP-1 T-CM or with serum-free DMEM and then incubated overnight. Cell debris was removed by centrifugation, and the collected supernatants were labeled as Mac-CM (DMEM treated) or MacT-CM (HKP1 T-CM treated). IL6 was measured by ELISA (R&D Systems) according to manufacturer's manual.

ACCESSION NUMBERS

The NCBI Gene Expression Omnibus (GEO) accession number for the RNA-seq reported in this paper is GSE59831.

SUPPLEMENTAL INFORMATION

Supplemental Information includes Supplemental Experimental Procedures, seven figures, and five tables and can be found with this article online at <http://dx.doi.org/10.1016/j.celrep.2015.01.040>.

AUTHOR CONTRIBUTIONS

H.C. and V.M. designed the study and wrote the manuscript. H.C. performed experiments. J.S., F.L., and S.T.C.W. developed the CCCEexplorer. D.G. and S.B.L. performed experiments and contributed to experiment design. O.E. analyzed RNA-seq data. N.N. examined tissue histology. A.D., S. Ryu, S. Rafii, and N.K.A. contributed to experimental design.

ACKNOWLEDGMENTS

We thank Jenny Xiang of the Genomics Resources Core Facility (WCMC) for the RNA sequencing and Dr. Tyler Jacks (MIT) with intratracheal delivery method training. This work was supported by funds from The Neuberger Berman Foundation Lung Cancer Center funds; the Arthur and Myra Mahon Donor-Advised Fund; the Liz Claiborne and Art Ortenberg Foundation; the R. & M. Goldberg Family Foundation; the P. & C. Collins Fund; the William and Shelby Modell Family Foundation Trust; generous funds donated by patients in the Division of Thoracic Surgery to V.M.; and grants to S.T.C.W. (NIH U54CA149196, NIH R01 CA121225, and John S. Dunn Research Foundation).

Received: July 18, 2014

Revised: December 7, 2014

Accepted: January 16, 2015

Published: February 19, 2015

REFERENCES

- Allinen, M., Beroukhim, R., Cai, L., Brennan, C., Lahti-Domenici, J., Huang, H., Porter, D., Hu, M., Chin, L., Richardson, A., et al. (2004). Molecular characterization of the tumor microenvironment in breast cancer. *Cancer Cell* 6, 17–32.
- Anastas, J.N., and Moon, R.T. (2013). WNT signalling pathways as therapeutic targets in cancer. *Nat. Rev. Cancer* 13, 11–26.
- Anders, S., and Huber, W. (2010). Differential expression analysis for sequence count data. *Genome Biol.* 11, R106.
- Anders, S., Theodor Pyl, P., and Huber, W. (2014). HTSeq—a Python framework to work with high-throughput sequencing data. Published online September 25, 2014. <http://dx.doi.org/10.1093/bioinformatics/btu638>.
- Anumanthan, G., Halder, S.K., Osada, H., Takahashi, T., Massion, P.P., Carbone, D.P., and Datta, P.K. (2005). Restoration of TGF-beta signalling reduces tumorigenicity in human lung cancer cells. *Br. J. Cancer* 93, 1157–1167.
- Barthelemy-Brichant, N., David, J.L., Bosquée, L., Bury, T., Seidel, L., Albert, A., Bartsch, P., Baugnet-Mahieu, L., and Deneufbourg, J.M. (2002). Increased TGFbeta1 plasma level in patients with lung cancer: potential mechanisms. *Eur. J. Clin. Invest.* 32, 193–198.
- Bellocq, A., Antoine, M., Flahault, A., Philippe, C., Crestani, B., Bernaudin, J.F., Mayaud, C., Milleron, B., Baud, L., and Cadranel, J. (1998). Neutrophil

- alveolitis in bronchioloalveolar carcinoma: induction by tumor-derived interleukin-8 and relation to clinical outcome. *Am. J. Pathol.* 152, 83–92.
- Blumenschein, G.R., Jr. (2012). Developmental antiangiogenic agents for the treatment of non-small cell lung cancer (NSCLC). *Invest. New Drugs* 30, 1802–1811.
- Busser, B., Sancey, L., Josserand, V., Niang, C., Khochbin, S., Favrot, M.C., Coll, J.L., and Hurbin, A. (2010). Amphiregulin promotes resistance to gefitinib in nonsmall cell lung cancer cells by regulating Ku70 acetylation. *Mol. Ther.* 18, 536–543.
- Chang, Q., Bournazou, E., Sansone, P., Berishaj, M., Gao, S.P., Daly, L., Wels, J., Theilen, T., Granitto, S., Zhang, X., et al. (2013). The IL-6/JAK/Stat3 feed-forward loop drives tumorigenesis and metastasis. *Neoplasia* 15, 848–862.
- Choi, Y.L., Soda, M., Yamashita, Y., Ueno, T., Takashima, J., Nakajima, T., Yatabe, Y., Takeuchi, K., Hamada, T., Haruta, H., et al.; ALK Lung Cancer Study Group (2010). EML4-ALK mutations in lung cancer that confer resistance to ALK inhibitors. *N. Engl. J. Med.* 363, 1734–1739.
- Chuang, H.Y., Lee, E., Liu, Y.T., Lee, D., and Ideker, T. (2007). Network-based classification of breast cancer metastasis. *Mol. Syst. Biol.* 3, 140.
- DeNardo, D.G., Brennan, D.J., Rexhepaj, E., Ruffell, B., Shiao, S.L., Madden, S.F., Gallagher, W.M., Wadhwan, N., Keil, S.D., Junaid, S.A., et al. (2011). Leukocyte complexity predicts breast cancer survival and functionally regulates response to chemotherapy. *Cancer Discov.* 1, 54–67.
- DuPage, M., Dooley, A.L., and Jacks, T. (2009). Conditional mouse lung cancer models using adenoviral or lentiviral delivery of Cre recombinase. *Nat. Protoc.* 4, 1064–1072.
- DuPage, M., Cheung, A.F., Mazumdar, C., Winslow, M.M., Bronson, R., Schmidt, L.M., Crowley, D., Chen, J., and Jacks, T. (2011). Endogenous T cell responses to antigens expressed in lung adenocarcinomas delay malignant tumor progression. *Cancer Cell* 19, 72–85.
- Franklin, R.A., Liao, W., Sarkar, A., Kim, M.V., Bivona, M.R., Liu, K., Pamer, E.G., and Li, M.O. (2014). The cellular and molecular origin of tumor-associated macrophages. *Science* 344, 921–925.
- Gao, S.P., Mark, K.G., Leslie, K., Pao, W., Motoi, N., Gerald, W.L., Travis, W.D., Bornmann, W., Veach, D., Clarkson, B., and Bromberg, J.F. (2007). Mutations in the EGFR kinase domain mediate STAT3 activation via IL-6 production in human lung adenocarcinomas. *J. Clin. Invest.* 117, 3846–3856.
- Gomis, R.R., Alarcón, C., Nadal, C., Van Poznak, C., and Massagué, J. (2006). C/EBPbeta at the core of the TGFbeta cytostatic response and its evasion in metastatic breast cancer cells. *Cancer Cell* 10, 203–214.
- Graeber, T.G., and Eisenberg, D. (2001). Bioinformatic identification of potential autocrine signaling loops in cancers from gene expression profiles. *Nat. Genet.* 29, 295–300.
- Guth, A.M., Janssen, W.J., Bosio, C.M., Crouch, E.C., Henson, P.M., and Dow, S.W. (2009). Lung environment determines unique phenotype of alveolar macrophages. *Am. J. Physiol. Lung Cell. Mol. Physiol.* 296, L936–L946.
- Hanahan, D., and Coussens, L.M. (2012). Accessories to the crime: functions of cells recruited to the tumor microenvironment. *Cancer Cell* 21, 309–322.
- Hart, T., Komori, H.K., LaMere, S., Podshivalova, K., and Salomon, D.R. (2013). Finding the active genes in deep RNA-seq gene expression studies. *BMC Genomics* 14, 778.
- Houghton, A.M., Rzymkiewicz, D.M., Ji, H., Gregory, A.D., Egea, E.E., Metz, H.E., Stoltz, D.B., Land, S.R., Marconcini, L.A., Kliment, C.R., et al. (2010). Neutrophil elastase-mediated degradation of IRS-1 accelerates lung tumor growth. *Nat. Med.* 16, 219–223.
- Hurbin, A., Dubrez, L., Coll, J.L., and Favrot, M.C. (2002). Inhibition of apoptosis by amphiregulin via an insulin-like growth factor-1 receptor-dependent pathway in non-small cell lung cancer cell lines. *J. Biol. Chem.* 277, 49127–49133.
- Ito, M., Ishii, G., Nagai, K., Maeda, R., Nakano, Y., and Ochiai, A. (2012). Prognostic impact of cancer-associated stromal cells in patients with stage I lung adenocarcinoma. *Chest* 142, 151–158.
- Joyce, J.A., and Pollard, J.W. (2009). Microenvironmental regulation of metastasis. *Nat. Rev. Cancer* 9, 239–252.
- Katoh, Y., and Katoh, M. (2006). Canonical WNT signaling pathway and human AREG. *Int. J. Mol. Med.* 17, 1163–1166.
- Kessenbrock, K., Plaks, V., and Werb, Z. (2010). Matrix metalloproteinases: regulators of the tumor microenvironment. *Cell* 141, 52–67.
- Kim, W.S., Park, C., Jung, Y.S., Kim, H.S., Han, J., Park, C.H., Kim, K., Kim, J., Shim, Y.M., and Park, K. (1999). Reduced transforming growth factor-beta type II receptor (TGF-beta RII) expression in adenocarcinoma of the lung. *Anticancer Res.* 19 (1A), 301–306.
- Komurov, K. (2012). Modeling community-wide molecular networks of multicellular systems. *Bioinformatics* 28, 694–700.
- Law, C.W., Chen, Y., Shi, W., and Smyth, G.K. (2014). voom: Precision weights unlock linear model analysis tools for RNA-seq read counts. *Genome Biol.* 15, R29.
- Li, H., Sorenson, A.L., Pocobutt, J., Amin, J., Joyal, T., Sullivan, T., Crossno, J.T., Jr., Weiser-Evans, M.C., and Nemenoff, R.A. (2011). Activation of PPARγ in myeloid cells promotes lung cancer progression and metastasis. *PLoS ONE* 6, e28133.
- Massagué, J. (2008). TGFbeta in Cancer. *Cell* 134, 215–230.
- Mortazavi, A., Williams, B.A., McCue, K., Schaeffer, L., and Wold, B. (2008). Mapping and quantifying mammalian transcriptomes by RNA-Seq. *Nat. Methods* 5, 621–628.
- Ogata, H., Goto, S., Sato, K., Fujibuchi, W., Bono, H., and Kanehisa, M. (1999). KEGG: Kyoto Encyclopedia of Genes and Genomes. *Nucleic Acids Res.* 27, 29–34.
- Oliveros, J.C. (2007). VENNY. an interactive tool for comparing lists with Venn Diagrams <http://bioinfogp.cnb.csic.es/tools/venny/index.html>.
- Pao, W., Miller, V.A., Politi, K.A., Riely, G.J., Somwar, R., Zakowski, M.F., Kris, M.G., and Varmus, H. (2005). Acquired resistance of lung adenocarcinomas to gefitinib or erlotinib is associated with a second mutation in the EGFR kinase domain. *PLoS Med.* 2, e73.
- Pyontek, S.M., Akkari, L., Schuhmacher, A.J., Bowman, R.L., Sevenich, L., Quail, D.F., Olson, O.C., Quick, M.L., Huse, J.T., Teijeiro, V., et al. (2013). CSF-1R inhibition alters macrophage polarization and blocks glioma progression. *Nat. Med.* 19, 1264–1272.
- Ruffell, B., Au, A., Rugo, H.S., Esserman, L.J., Hwang, E.S., and Coussens, L.M. (2012). Leukocyte composition of human breast cancer. *Proc. Natl. Acad. Sci. USA* 109, 2796–2801.
- Schafer, Z.T., and Brugge, J.S. (2007). IL-6 involvement in epithelial cancers. *J. Clin. Invest.* 117, 3660–3663.
- Seder, C.W., Hartojo, W., Lin, L., Silvers, A.L., Wang, Z., Thomas, D.G., Giordano, T.J., Chen, G., Chang, A.C., Orringer, M.B., and Beer, D.G. (2009). Upregulated INHBA expression may promote cell proliferation and is associated with poor survival in lung adenocarcinoma. *Neoplasia* 11, 388–396.
- Sethi, T., Rintoul, R.C., Moore, S.M., MacKinnon, A.C., Salter, D., Choo, C., Chilvers, E.R., Dransfield, I., Donnelly, S.C., Strieter, R., and Haslett, C. (1999). Extracellular matrix proteins protect small cell lung cancer cells against apoptosis: a mechanism for small cell lung cancer growth and drug resistance in vivo. *Nat. Med.* 5, 662–668.
- Shree, T., Olson, O.C., Elie, B.T., Kester, J.C., Garfall, A.L., Simpson, K., Bell-McGuinn, K.M., Zabor, E.C., Brogi, E., and Joyce, J.A. (2011). Macrophages and cathepsin proteases blunt chemotherapeutic response in breast cancer. *Genes Dev.* 25, 2465–2479.
- Siegel, R., Ma, J., Zou, Z., and Jemal, A. (2014). Cancer statistics, 2014. *CA Cancer J. Clin.* 64, 9–29.
- Smyth, M.J., Hayakawa, Y., Takeda, K., and Yagita, H. (2002). New aspects of natural-killer-cell surveillance and therapy of cancer. *Nat. Rev. Cancer* 2, 850–861.
- Solis, L.M., Behrens, C., Raso, M.G., Lin, H.Y., Kadara, H., Yuan, P., Galindo, H., Tang, X., Lee, J.J., Kalhor, N., et al. (2012). Histologic patterns and molecular characteristics of lung adenocarcinoma associated with clinical outcome. *Cancer* 118, 2889–2899.

- Standiford, T.J., Kuick, R., Bhan, U., Chen, J., Newstead, M., and Keshamouni, V.G. (2011). TGF- β -induced IRAK-M expression in tumor-associated macrophages regulates lung tumor growth. *Oncogene* 30, 2475–2484.
- Sugimoto, H., Mundel, T.M., Kieran, M.W., and Kalluri, R. (2006). Identification of fibroblast heterogeneity in the tumor microenvironment. *Cancer Biol. Ther.* 5, 1640–1646.
- Szklarczyk, D., Franceschini, A., Kuhn, M., Simonovic, M., Roth, A., Minguez, P., Doerks, T., Stark, M., Muller, J., Bork, P., et al. (2011). The STRING database in 2011: functional interaction networks of proteins, globally integrated and scored. *Nucleic Acids Res.* 39, D561–D568.
- Toonkel, R.L., Borczuk, A.C., and Powell, C.A. (2010). Tgf-beta signaling pathway in lung adenocarcinoma invasion. *J. Thorac. Oncol.* 5, 153–157.
- Wang, R., Zhang, J., Chen, S., Lu, M., Luo, X., Yao, S., Liu, S., Qin, Y., and Chen, H. (2011). Tumor-associated macrophages provide a suitable microenvironment for non-small lung cancer invasion and progression. *Lung Cancer* 74, 188–196.
- Warnes, G.R., Bolker, B., Bonebakker, L., Gentleman, R., Liaw, W.H.A., Lumley, T., Maechler, M., Magnusson, A., Moeller, S., Schwartz, M., et al. (2014). gplots: Various R programming tools for plotting data. <http://cran.r-project.org/web/packages/gplots/index.html>.
- Weischenfeldt, J., and Porse, B. (2008). Bone marrow-derived macrophages (BMM): isolation and applications. *CSH Protoc.* 2008, pdb.prot5080.
- Welsh, T.J., Green, R.H., Richardson, D., Waller, D.A., O'Byrne, K.J., and Bradding, P. (2005). Macrophage and mast-cell invasion of tumor cell islets confers a marked survival advantage in non-small-cell lung cancer. *J. Clin. Oncol.* 23, 8959–8967.
- Wyckoff, J., Wang, W., Lin, E.Y., Wang, Y., Pixley, F., Stanley, E.R., Graf, T., Pollard, J.W., Segall, J., and Condeellis, J. (2004). A paracrine loop between tumor cells and macrophages is required for tumor cell migration in mammary tumors. *Cancer Res.* 64, 7022–7029.
- Xu, C.C., Wu, L.M., Sun, W., Zhang, N., Chen, W.S., and Fu, X.N. (2011). Effects of TGF- β signaling blockade on human A549 lung adenocarcinoma cell lines. *Mol. Med. Rep.* 4, 1007–1015.
- Zhong, Z., Wen, Z., and Darnell, J.E., Jr. (1994). Stat3: a STAT family member activated by tyrosine phosphorylation in response to epidermal growth factor and interleukin-6. *Science* 264, 95–98.